Temperature-dependent electronic structure, spin-resolved photoemission, and magnetic dichroism of ultrathin ferromagnetic films: Co/Cu(001)

2001 J. Phys.: Condens. Matter 13 833

(http://iopscience.iop.org/0953-8984/13/5/305)

INSTITUTE OF PHYSICS PUBLISHING JOURNAL OF PHYSICS: CONDENSED MATTER

J. Phys.: Condens. Matter **13** (2001) 833–849 www.iop.org/Journals/cm PII: S0953-8984(01)17669-1

Temperature-dependent electronic structure, spin-resolved photoemission, and magnetic dichroism of ultrathin ferromagnetic films: Co/Cu(001)

J Henk

Max-Planck-Institut für Mikrostrukturphysik, Weinberg 2, D-06120 Halle (Saale), Germany

E-mail: henk@mpi-halle.mpg.de

Received 4 October 2000, in final form 8 December 2000

Abstract

The temperature dependences of the electronic structure, spin-resolved photoemission, and magnetic linear dichroism of the prototypical system 2 ML Co on Cu(001) (ML stands for monolayer(s)) are presented in a detailed theoretical study. Relativistic *ab initio* electronic structure calculations were carried out within the framework of multiple-scattering theory; the spin-resolved photoemission was calculated within the one-step model. The temperature dependence was taken into account within the disordered local moment picture.

The spectral features show a distinct dispersion and broadening with temperature, in particular those derived from quantum-well states in the Co film. These findings can be traced back to the layer- and spin-resolved Bloch spectral function. Further, Co-derived maxima in the photoemission intensities behave significantly differently with temperature to Cu-derived ones. The spin-resolved photoemission intensities compare well with experimental data and with theoretical data obtained within the fluctuating local moment picture. Magnetic linear dichroism in spin-resolved photoemission is discussed in terms of asymmetries which are related to the spin polarizations.

1. Introduction

Joint experimental and theoretical investigations of solids, in particular those of 3d ferromagnets, by photoelectron spectroscopy have proved to be very successful and allowed detailed statements to be made as regards the spin- and symmetry-resolved electronic structure (see for example [1]). Theoretical photoemission calculations are—like the underlying *ab initio* band-structure calculations—usually performed for zero temperature. The corresponding experiments, however, are carried out at elevated temperatures, e.g. at room temperature. Theoretical and experimental photoemission spectra agree well in general for ferromagnetic systems with the Curie temperatures T_C which are high compared to the actual temperature at which the experiments were performed. However, the agreement is rather poor for systems with low Curie temperatures, for example ultrathin films. For two monolayers (ML) of Co on

0953-8984/01/050833+17$30.00

Cu(001), T_C was estimated at only 320 K [2], as compared to a bulk T_C of 1388 K [3] (Huang *et al* found a value of about 500 K by means of the surface magneto-optic Kerr effect [4]). In order to overcome this temperature 'mismatch' between theory and experiment, one can either cool the samples in experiment down to temperatures close enough to zero or extend the theory to non-zero temperatures—obviously a far better approach. The latter allows detailed studies of the temperature dependence of significant electron-spectroscopic quantities: for example magnetic moments, spin polarization, and magnetic dichroism (MD) in photoemission.

Temperature effects can be divided into vibrational and electronic effects. The former, i.e. phonons, are treated in multiple-scattering theories of electron spectroscopies (e.g. low-energy electron diffraction (LEED) and photoemission) via temperature-dependent scattering phase shifts (see for example [5, 6]). The electronic temperature effects can be taken into account by an energy-, spin-, and temperature-dependent self-energy Σ which can be approached in different ways. In a first approach, one can combine density-functional theory and many-body treatments. For example, a Hubbard-type multiband model allows the computation of spin-resolved photoemission spectra within a generalized one-step model [7–9]. For low-index surfaces of Ni the comparison of spectra calculated within this framework showed good agreement with experimental data. No indication of a stationary exchange splitting independent of temperature could be found. Instead, majority and minority spin states merged in energy upon approaching T_C. Another treatment is based on a periodic cluster approach with exact diagonalization of the many-particle Hamiltonian for ultrathin transition-metal films [10].

A further approach is based on the coherent potential approximation (CPA) [11] as formulated in the Korringa–Kohn–Rostoker (KKR) method [12–14]. The disorder in the solid gives rise to the electron self-energy operator Σ [15]. Therefore, the electronic structure has to be described by means of the Bloch spectral function (BSF) $A_B(E, \boldsymbol{k})$ (i.e. the energy- and wavevector-resolved density of states) instead of by means of the more familiar band structure $E(\boldsymbol{k})$. The real part of Σ shifts the energy levels (e.g. defined as maxima in $A_B(E, \boldsymbol{k})$); its imaginary part gives rise to broadening, i.e. to a finite lifetime of the quasi-particles. The CPA can be used for binary substitutional alloys A_xB_{1-x} to formulate a first-principles theory of phase transitions in ferromagnets [16, 17]: in the disordered local moment (DLM) picture, one identifies the atomic species A and B as atoms of the same kind but with opposite orientations of the local magnetic moment $\boldsymbol{M}$: $\boldsymbol{M}_A = -\boldsymbol{M}_B$. For given concentration x and energy E, an effective medium is computed, which is determined by the condition that inserting a defect of type A weighted with its concentration x and inserting a defect of type B weighted with its concentration $1 - x$ into the effective medium imposes no additional scattering (for details see references [14, 15]). For example, for concentration $x = 0$ all local magnetic moments are aligned parallel and one has the ferromagnetic case for $T = 0$, since all sites are occupied by atoms of species B. For $x = 0.5$ the net magnetization vanishes due to there being equal numbers of sites occupied by species A and B; hence one is concerned with the paramagnetic case for $T = T_C$. A theory of photoemission from binary substitutional alloys has been formulated by Durham [18] and successfully applied within the DLM picture to Fe at elevated temperatures [19].

If the CPA calculations are performed within the single-site approximation, magnetic short-range order (SRO), i.e. correlation between the local magnetic moments, is neglected (note that within the embedded-cluster method, SRO can of course be treated [20]). In order to take into account the spin–spin correlations, Haines *et al* [21, 22] proposed the fluctuating local moment (FLM) picture which uses clusters with a magnetic moment located at each site. The configurations of local magnetic moments have to be compatible with a given average magnetic moment $\langle m(T) \rangle$ and a spin–spin correlation length $\Lambda(T)$ [23]. Physical quantities are then

obtained by averaging over the configurations. Gollisch and Feder applied this approach successfully to photoemission from Ni(111) and Fe_3Pt [24–26]. The joint effect of lattice vibrations and magnetic fluctuations in Ni has been investigated by Delgadillo *et al* [27].

As mentioned above, ultrathin films show a low T_C with respect to the bulk system. Thus, significant temperature effects on spin-resolved photoemission intensities can be expected even at room temperature. Reiser *et al* [28] investigated theoretically 2 ML Co on Cu(001) within the FLM theory and found good agreement with experiment at $T = 0.65\,T_C$ [29] for a certain pair of average magnetic moment and correlation length ($\langle m(T)\rangle = 0.2\,m(0)$ and $\Lambda(T)$ less than the intersite distance). However, they applied an empirical tight-binding description of the electronic structure and did not take into account spin–orbit coupling (SOC), an essential ingredient for the description of magnetic dichroism (MD) in photoemission, i.e. the change of the photocurrent upon reversal of the magnetization orientation [30]. Hence, there appears to be a need for a theoretical investigation of the temperature dependences of the electronic structure, spin-resolved photoemission, and MD from ultrathin films. Its basis should be an *ab initio* electronic structure calculation which treats exchange and spin–orbit interactions on an equal footing. In this paper we present results of such an investigation by means of the fully relativistic layer-KKR method but within the DLM picture instead of the FLM picture. As a prototypical system we chose 2 ML Co/Cu(001) and address further the temperature dependence of the magnetic linear dichroism (MLD) in valence band photoemission. Since we are dealing with spin-resolved MLD, we introduce asymmetries which turn out to be related to the exchange- and the spin–orbit-induced photoelectron spin polarizations (ESPs). In recent works the temperature dependence of the MD has been exclusively (at least to our knowledge) investigated in an element-specific way, exploiting core levels [31, 32]. Further, Alders *et al* presented a joint experimental and theoretical study of the spin–spin correlation function and magnetic long-range order in x-ray absorption in NiO [33].

This paper is organized as follows. In section 2 we sketch the theoretical methods, in particular the numerical details (section 2.1) and the asymmetries (section 2.2). Results are presented and discussed in section 3, in particular for the electronic structure (section 3.1), photoemission (section 3.2), and magnetic linear dichroism (section 3.3). Concluding remarks are made in section 4.

2. Theoretical aspects

2.1. Numerical details

As a prototypical system we chose 2 ML Co on Cu(001) in order to allow comparison of our results with experiment [29] and previous theoretical results [28]. Cobalt grows in a layer-by-layer mode on Cu(001) and continues the fcc Cu lattice but with a slight tetragonal distortion (for growth of Co on Cu(001), see for example [34–36]). In our calculations we did not take into account any tetragonal distortion at the surface, but assumed the fcc parent Cu lattice to extend throughout the whole semi-infinite system. Nor do we consider Cu–Co intermixing at the interface. The layers are denoted as S, S − 1, S − 2, ..., starting from the outermost surface layer. Bulk layers are denoted by B.

As the first step of the calculations, spin-dependent muffin-tin potentials $V_{\pm}(r)$ were self-consistently determined by the spin-polarized scalar-relativistic layer-KKR method (within the local spin-density approximation of density-functional theory). We used the exchange–correlation potential of Perdew and Wang [37]. At this step, spin–orbit coupling (SOC) was not taken into account. For maximum angular momentum $l_{max} = 3$, the magnetic moments of the Co sites are $m(S) = 1.79\ \mu_B$ and $m(S-1) = 1.62\ \mu_B$. These values

correspond to changes of +7.8% and −2.4% of the bulk moment ($m(\mathrm{B}) = 1.66\ \mu_\mathrm{B}$) and compare well with those obtained by other self-consistent methods (Clemens *et al* give $m(\mathrm{S}) = 1.84\ \mu_\mathrm{B}$ and $m(\mathrm{S}-1) = 1.60\ \mu_\mathrm{B}$ [29]; Niklasson gives $m(\mathrm{S}) = 1.81\ \mu_\mathrm{B}$, $m(\mathrm{S}-1) = 1.61\ \mu_\mathrm{B}$, and $m(\mathrm{B}) = 1.68\ \mu_\mathrm{B}$ [38]). The induced spin moment in the adjacent Cu layer is $m(\mathrm{S}-2) = 0.02\ \mu_\mathrm{B}$. We found no significant charge transfer from Co to Cu. The spin-dependent potentials $V_\pm$ serve as input for the fully relativistic layer-KKR calculations.

The description of magnetic dichroism in photoemission—one of the aims in this investigation—has to deal with both SOC and exchange splitting, which are best treated on an equal footing. Therefore, we applied in the second step the spin-polarized relativistic layer-KKR method [39] in order to determine the layer-resolved Green function, the most important quantity in electronic structure and photoemission calculations, from which all observables can be calculated. Following the ideas of the DLM picture, the electronic temperature effects are treated within the inhomogeneous CPA for binary substitutional alloys [16, 17]. As input for atomic species A we took the spin-dependent potentials from the first step, for species B the same but with opposite spin orientation (i.e. $V_\pm^\mathrm{A} = V_\mp^\mathrm{B}$; thus $\boldsymbol{M}_\mathrm{A} = -\boldsymbol{M}_\mathrm{B}$). For concentration $x = 0$ the layer- and spin-resolved Bloch spectral functions (BSFs) obtained from the fully relativistic and the scalar-relativistic calculations agreed almost perfectly. The slight deviations can unambiguously be attributed to the inclusion of SOC in the former, as can easily be checked by scaling the SOC while keeping the other relativistic effects unchanged [40, 41].

For selected concentrations x ranging from 0 ($T = 0$) to 0.5 ($T = T_\mathrm{C}$), we calculated from the Green function the layer- and spin-resolved BSF $A_\mathrm{B}(E, \boldsymbol{k}_\parallel)$ and the spin-resolved photoemission intensities within the one-step model following the work of Durham *et al* [19]. Instead of treating the photoelectron state, i.e. the time-reversed spin-polarized LEED state, within the averaged t-matrix approximation (ATA), we treated it like the hole state within the CPA because of the rather small number of CPA self-consistency iterations required. Additionally, the CPA results were compared with those obtained within the virtual-crystal approximation (VCA) and the ATA. The ATA yielded the same general trends as the CPA but the results at certain energies differed significantly. As expected, the VCA results did not agree well with those obtained within the CPA or with those obtained within the ATA.

Finally, we present some technical details. From the layer-dependent 'impurity matrices' D^A and D^B (see for example [13]), the configurationally averaged D^C was obtained from $D^\mathrm{C} = xD^\mathrm{A} + (1-x)D^\mathrm{B}$, from which the effective single-site t-matrices of the coherent system were calculated. Starting from the ATA t-matrices we did not encounter any convergence problems in the CPA self-consistency loop. Further, the averaging over reciprocal space was carefully checked, applying both special-point sets as well as self-adapting grid methods (see for example [42]). Note that the Fermi energy E_F is independent of the concentration x because it is fixed by the non-magnetic Cu substrate.

Many-particle effects play an important role for transition metals, one prominent example being the 6 eV satellite for Ni. These effects are expected to be larger in systems with reduced dimensionality, e.g. ultrathin films, than in bulk systems. In a series of publications (see for example references [43–45]), Chen investigated in detail many-particle effects in ultrathin Co films within a non-perturbative many-body approach [46]. One of the main results was the importance of hybridization between the Co d states of the film and the Cu s states of the substrate [10]. The photoemission intensity of a strong satellite peak in the theoretical spectra was considerably reduced if the Co d/Cu s hybridization was taken into account, thus improving the agreement between experiment [29] and theory. Further, many-body effects showed up as a transfer of spectral weight to lower energies than predicted by a single-particle approach (in particular at energies $E < -5.2$ eV).

Such sophisticated many-body calculations are beyond the scope of our investigation. Instead, in our single-particle calculations we model many-particle effects via an energy-dependent optical potential. In the calculations of the BSF a constant imaginary part of the energy of 0.025 eV was used. In the photoemission calculations the hole lifetimes were simulated via an energy-dependent imaginary part of the energy of Im $E = 0.1(E - E_F)$ for Co layers and Im $E = 0.025(E - E_F)$ for Cu layers. For the photoelectron states a constant value of 3.5 eV was taken (note that due to the larger imaginary parts in the photoemission calculations, a slight shift of the electronic states to higher energies with respect to the BSF calculations occurs). Further, the photoemission intensities were collected from the first 20 outermost layers, the maximum angular momentum was $l_{max} = 4$, and the number of reciprocal-lattice vectors was about 50. Fresnel's equations and Snell's law were not taken into account.

We wish to stress that our aim was to investigate the basic temperature effects on photoemission and magnetic dichroism. Therefore, we did not optimize the above parameters in order to achieve perfect agreement with experiment. However, in future work we shall incorporate the self-energy Σ within the GW approximation [47–49]. This would account for changes in both the layer- and energy-dependent exchange splitting and in the quasi-particle lifetimes via Re Σ and Im Σ, respectively.

Finally, we briefly compare the approach of Nolting *et al* [9] with the DLM approach. In the former, one first computes the electronic band structure of the paramagnetic bulk system. This is used in a second step as input for a Hubbard-type many-particle model with Coulomb and exchange parameters U and J, respectively. The latter are chosen to reproduce the ground-state magnetization at $T = 0$ K. The resulting set of equations is solved self-consistently and yields the energy-, spin-, and temperature-dependent self-energy for the occupied states. In a third step, the spin-resolved photocurrent is calculated in a generalized one-step model of photoemission, in which the many-particle effects are taken into account only for the occupied states. This approach has the advantage (like that of Chen [10]) that correlations are accounted for in a sophisticated manner. In the DLM approach, however, these are considered in a rather rudimentary form (see above). In favour of the DLM approach one can say that it can easily be applied to ultrathin films (since it does not rely on bulk properties), that the temperature dependence is considered for both occupied states and the photoelectron state, and that additional parameters do not enter.

2.2. Asymmetries for magnetic dichroism in spin-resolved photoemission

In the following we introduce the asymmetries used in the discussion of magnetic linear dichroism (MLD) in spin-resolved photoemission (see section 3.3 below). In an experiment or a calculation for magnetic dichroism, one records the photocurrent I as a function of the magnetization orientation, $I(\pm\boldsymbol{M})$. If the photocurrent is further spin-analysed ($\pm\sigma$) with respect to the direction of $+\boldsymbol{M}$, one is concerned with a set of four spectra, $I(\pm\sigma, \pm\boldsymbol{M})$, or for short, $I_{\pm\pm}$.

The electron spin polarization (ESP) can be decomposed into an even part and an odd part in terms of $\boldsymbol{M}$: $P(\boldsymbol{M}) = P_{ex}(\boldsymbol{M}) + P_{so}(\boldsymbol{M})$, with $P_{ex}(\boldsymbol{M}) = -P_{ex}(-\boldsymbol{M})$ and $P_{so}(\boldsymbol{M}) = P_{so}(-\boldsymbol{M})$. In terms of the intensities, these ESPs are given by

$$\begin{aligned} P_{so} &= \frac{I_{++} - I_{-+}}{2I_+} + \frac{I_{+-} - I_{--}}{2I_-} \\ P_{ex} &= \frac{I_{++} - I_{-+}}{2I_+} - \frac{I_{+-} - I_{--}}{2I_-} \end{aligned} \tag{1}$$

with the spin-averaged intensities $I_\mu = \sum_\sigma I_{\sigma\mu}$. Vice versa, the intensities can be written as

$$I_{\sigma\mu} = \frac{1}{2}\left[1 + \sigma(P_{\mathrm{so}} + \mu P_{\mathrm{ex}})\right] I_\mu \qquad \sigma, \mu = \pm. \tag{2}$$

The origins of the ESP contributions become evident on considering the following limiting cases for $I_+ = I_-$. If there is no magnetization ($M = 0$) the ESP is exclusively due to SOC ($P_{\mathrm{so}} \neq 0$ and $P_{\mathrm{ex}} = 0$). If on the other hand there is no SOC, the polarization changes sign upon reversal of M ($P_{\mathrm{ex}} \neq 0$ and $P_{\mathrm{so}} = 0$). In short, P_{ex} can be attributed to exchange splitting, P_{so} to SOC.

The four intensities $I_{\pm\pm}$ allow the definition of three asymmetries:

$$\begin{aligned} A_{\mathrm{un}} &= \frac{1}{I_0}(I_{++} + I_{-+} - I_{+-} - I_{--}) \\ A_{\mathrm{so}} &= \frac{1}{I_0}(I_{++} - I_{-+} + I_{+-} - I_{--}) \\ A_{\mathrm{ex}} &= \frac{1}{I_0}(I_{++} - I_{-+} - I_{+-} + I_{--}) \end{aligned} \tag{3}$$

with the total current $I_0 = \sum_{\sigma\mu} I_{\sigma\mu}$, which in terms of the ESPs can be compactly written as

$$\begin{aligned} A_{\mathrm{un}} &= \frac{1}{I_0}(I_+ - I_-) \\ A_{\mathrm{so}} &= P_{\mathrm{so}} + P_{\mathrm{ex}} A_{\mathrm{un}} \\ A_{\mathrm{ex}} &= P_{\mathrm{ex}} + P_{\mathrm{so}} A_{\mathrm{un}}. \end{aligned} \tag{4}$$

There is no dichroism ($A_{\mathrm{un}} = 0$) if there is either no exchange splitting or no SOC. In the first case, $I_{\pm\pm} = I_{\pm\mp}$ leads to $P_{\mathrm{ex}} = 0$ and, thus, $A_{\mathrm{ex}} = 0$ but $A_{\mathrm{so}} = P_{\mathrm{so}}$. In the second case, $I_{\pm\pm} = I_{\mp\mp}$ leads to $P_{\mathrm{so}} = 0$ and $A_{\mathrm{so}} = 0$ but $A_{\mathrm{ex}} = P_{\mathrm{ex}}$. Now consider 'perfect' dichroism, i.e. $A_{\mathrm{un}} = \pm 1$. For $A_{\mathrm{un}} = 1$ one has $I_+ \neq 0$, $I_- = 0$, and $A_{\mathrm{so}} = A_{\mathrm{ex}} = P_{\mathrm{so}} + P_{\mathrm{ex}}$; for $A_{\mathrm{un}} = -1$, $I_+ = 0$, $I_- \neq 0$, and $A_{\mathrm{so}} = -A_{\mathrm{ex}} = P_{\mathrm{so}} - P_{\mathrm{ex}}$. In conclusion, A_{un} is the commonly used spin-averaged asymmetry, whereas A_{so} and A_{ex} probe asymmetries which can be attributed to SOC and exchange splitting, respectively, if the dichroism is rather small. The asymmetries defined above can thus be regarded as generalizations of spin polarizations to the case of magnetic dichroism.

Sometimes it is stated that MD can be used as a substitute for spin-resolved measurements (for a discussion see [50]), possibly with the ulterior motive of achieving information on the spin polarization P_{ex} from the spin-averaged asymmetry A_{un} (the apparent advantage of MD measurements is the much higher count rate with respect to that in spin-resolved experiments). Considering (4), this is impossible, because the three asymmetries are linearly independent. Further, the expression for A_{un} contains neither P_{ex} nor P_{so}. Therefore, in order to obtain the ESP one has to measure A_{ex} or A_{so}, which requires spin resolution. Nevertheless, we shall briefly analyse our results for spin-resolved MLD with regard to the relations of the asymmetries to the ESPs (see section 3.3 below).

3. Results and discussion

In the following we present and discuss results for 2 ML fcc Co on Cu(001) which have been obtained by the spin-polarized relativistic layer-KKR method sketched in section 2.1. First, we turn to the electronic valence band structure which is essential for understanding the photoemission results (sections 3.2 and 3.3).

3.1. Electronic structure of 2 ML Co on Cu(001)

In figure 1 the spin- and layer-resolved Bloch spectral function $A_B(E, \boldsymbol{k}_\parallel)$ is shown for $\boldsymbol{k}_\parallel = 0$ and concentration x varied from 0 ($T = 0$) to 0.5 ($T = T_C$). Due to SOC, spin is not a good quantum number and, hence, the spin polarization of individual states is not equal to ± 1. Despite this, we use the terms 'majority' and 'minority' because in general the spin polarization is rather close to +1 (majority) or -1 (minority). Exceptions are for example states near spin–orbit-induced band gaps (see e.g. [51]).

We first address the case $x = 0$; cf. the uppermost curves in figure 1.

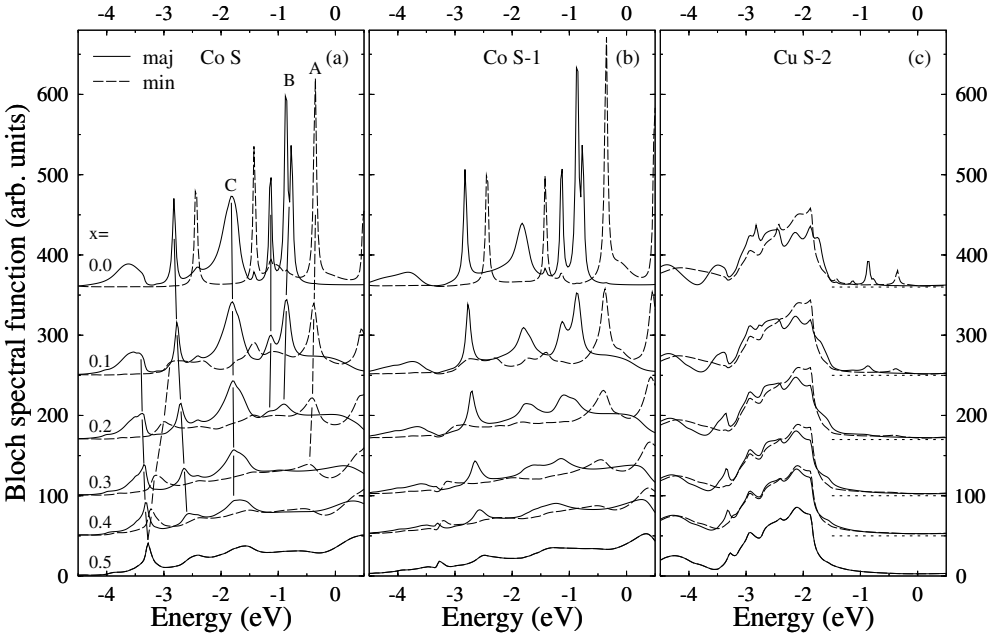

Figure 1. The spin- and layer-resolved Bloch spectral function of 2 ML Co on Cu(001) for $\boldsymbol{k}_\parallel = 0$ and concentrations $x = 0.0, \ldots, 0.5$, as indicated in (a). Majority-spin ('maj', ——) and minority-spin ('min', - - - -) projections are shown for the three outermost layers: Co S (a), Co S − 1 (b), and Cu S − 2 (c). In (a) maxima discussed in the text are connected by lines to guide the eye, three of them labelled A, B, and C. The respective zero abscissae are marked by dotted (· · · · · ·) lines in (c). The Fermi energy is 0 eV. For $x = 0.5$, the majority and minority curves coincide.

Due to the reflection at the Co/Cu interface and at the surface barrier, electrons become confined to the Co film and thus show up as spin-split quantum-well states (QWSs) and quantum-well resonances in the Co layers S and S − 1 (cf. panels (a) and (b)). Within the sp-band range of Cu, i.e. at energies larger than ≈ -1.8 eV, there is a strong minority state at -0.35 eV (labelled A in panel (a)). A majority double maximum is found at -0.78 eV and -0.84 eV (labelled B). Distinct traces of these QWSs are visible in the adjacent Cu layer S − 2 (panel (c)). Another important majority-spin state is indicated by the rather broad maximum at -1.83 eV which is resonant with the d bands of Cu (labelled C). The spin polarization of the individual states in the Co film can easily be derived from the bulk band structure of fcc Co [52].

With increasing concentration x the sharp maxima become smeared out, which can be explained by the CPA. Within this approximation, the BSF is given by a sum of concentration-weighted terms which either depend explicitly on the actual $\boldsymbol{k}_\parallel$ or which include averaging

over reciprocal space [14, 15]. For $x = 0$ the $\boldsymbol{k}_\parallel$-averaged terms cancel and one is left with the sharp maxima at $\boldsymbol{k}_\parallel = 0$. Upon increasing x the $\boldsymbol{k}_\parallel$-averaged terms become mixed in and thus lead to broadening of the peaks.

The Co states within the Cu sp-band range become rather continuously smeared out with increasing x. However, there are states whose BSF depends strongly on the concentration. For example the minority state at -2.45 eV (panel (a)) shows a high density of states for $x = 0$ but has practically disappeared for $x = 0.1$. Its majority partner at -2.83 eV, however, can be traced even up to $x = 0.4$ (cf. the guiding lines in panel (a)). On the other hand, one can find states which show sharp maxima for $x = 0.5$ but broad ones at $x = 0.0$, for example in layer S the peak at -3.28 eV.

For $x = 0.5$ the spin polarization of all layers vanishes because the net magnetic moment is zero ($T = T_C$, paramagnetic case). In a Stoner-type model one would expect majority and minority maxima to merge with decreasing exchange splitting. The maxima in the BSF do indeed show a slight dispersion with x (cf. the lines to guide the eye in panel (a)). Majority maxima disperse to higher energies, minority ones to lower energies, as expected. A very clear example of peak merging is found in layer S at -3.28 eV for $x = 0.5$: with decreasing x this maximum splits into two with opposite spin orientations. Note that the dispersion is non-symmetric, i.e. the majority peak shows less dispersion than its minority partner ($\approx$0.12 eV versus $\approx$0.38 eV). This behaviour can be attributed to the Cu band structure. The latter affects the reflection properties at the Co/Cu interface—in particular the phase shift—in a spin- and energy-dependent manner [53]. These reflection properties determine the energy positions of the QWSs: viewing the Co film as an interferometer [54], a QWS occurs at an energy at which the round-trip criterion is fulfilled, i.e. the phase accumulated in a round-trip is an even multiple of π. There are no further sharp maxima in layers S and S $-$ 1 for $x = 0.5$. The individual peaks at $x = 0$ cannot be traced well to $x = 0.5$ because of the broadening and decay of the spectral weight upon increasing x. However, from figure 1 it is evident that there is dispersion with x, but it is difficult to strictly evidence merging of maxima.

Summing up, our results for the spin- and layer-resolved BSF at various concentrations x reveal splitting, broadening, and in some cases merging of individual electronic states in the Co film. The individual maxima show a rather different behaviour as regards the spectral weight: some depend rather strongly on x, while others do not. In the following we turn to the temperature dependence of the photoemission and discuss whether the findings for the BSF can also be observed in the spin-resolved intensities.

3.2. Spin-resolved photoemission from 2 ML Co on Cu(001)

Spin-resolved experimental data for 2.5 ML Co/Cu(001) were recorded for s-polarized light at 45 eV photon energy and normal emission ($\boldsymbol{k}_\parallel = 0$) by Clemens *et al* [29] (cf. the bottom spectra in figure 2). The spectra were taken at room temperature, which corresponds to $T \approx 0.65\ T_C$ with T_C(2.5 ML) $\approx$ 465 K according to [2]. Note that in this set-up there is no magnetic dichroism because P_{so} vanishes [55]. The main question that arises is that of whether our theoretical approach which neglects magnetic SRO is able to reproduce the experimental data or whether magnetic SRO has to be taken into account.

In the current set-up the electric field vector of the s-polarized light is parallel to the surface plane and lies within a mirror plane of the solid. Therefore, only transitions from initial states of the representations $\Delta_5^\pm$ to the $\Delta_1^\pm$ final states are allowed [55] (here we prefer the more familiar but strictly speaking incorrect notation of single-group representations combined with a spin index instead of that of magnetic double groups).

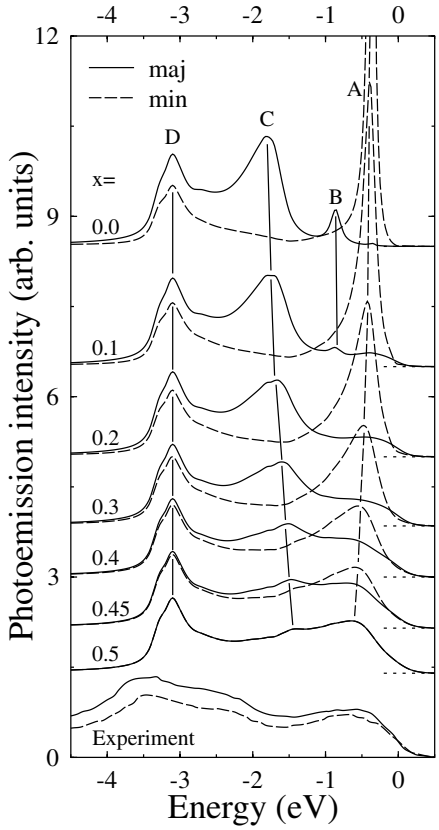

Figure 2. Spin-resolved photoemission intensities for 2 ML Co on Cu(001) for normal emission ($\boldsymbol{k}_\parallel = 0$) and concentrations $x = 0.0, \ldots, 0.5$. The photon energy of the s-polarized light is 45 eV. Majority ('maj') and minority ('min') spin projections are indicated by full (——) and dashed (- - - -) lines, respectively, whereas the zero abscissae are marked by dotted (· · · · · ·) lines. Maxima discussed in the text are denoted as A–D; almost vertical lines serve to guide the eye. The experimental spectra for 2.5 ML Co on Cu(001) were taken at room temperature (reproduced from [29]). Note that there is no magnetic dichroism in this set-up. The Fermi energy is 0 eV.

Before discussing the ESP in more detail we have to sketch its origins. As mentioned above, the spin–orbit-induced part P_{so} of the ESP vanishes in the current set-up and we are therefore concerned only with its exchange-induced part P_{ex}. The valence electrons in the Co film are spin polarized and this polarization is transferred in the excitation process to that of the outgoing photoelectrons (note that the ESP of the photoelectrons is *not* identical to those of the valence electrons, due to matrix-element effects). The valence electrons in the Cu substrate, however, are not spin polarized, and, hence, neither are the photoelectrons in the substrate. These photoelectrons have to pass the magnetic Co film on their path to the detector, and the spin-dependent transmission of the latter induces a spin polarization of the outgoing electrons. In turn, if one produces spin-polarized photoelectrons in the non-magnetic substrate, e.g. by optical orientation, the magnetic film can be exploited as a spin detector [56]. Summing up, the spatial origin of the photoelectrons—either the Co film or the Cu substrate—is reflected by two different mechanisms for producing ESP. And further, the latter should differ considerably in their temperature dependence since in the first case both initial and final states are affected by T whereas in the other only the final states are affected.

The top curves in figure 2 are theoretical spin-resolved spectra for concentration $x = 0$. At -0.35 eV the minority QWS A (cf. panel (a) in figure 1) gives rise to a very strong intensity maximum, whereas the majority QWS B at -0.84 eV shows up as a comparably small peak (the 'matrix-element effect'). The rather broad majority maximum C at -1.85 eV is related to that in the BSF. In contrast to these spectral features which show strong ESP, the maximum D at -3.10 eV contains considerable contributions from both spin orientations. Since the BSF at this energy is very small in the Co layers but comparably large in the Cu layers, it seems likely that D is due to emission from the Cu substrate. Its spin polarization can thus be attributed to the Co-induced magnetic moments in the Cu layers at the Co/Cu interface or to the spin-dependent transmission of the photoelectron through the Co film ('spin filter'). But since the magnetic moment induced in Cu layer $S - 2$ is too small ($0.02\ \mu_B$) to be regarded as responsible for the D ESP of about 20%, the ESP can be attributed unambiguously to the spin-dependent transmission through the Co film.

The origin of peak D becomes even more evident when considering the temperature dependence of the intensity: with increasing concentration x there is no shift in energy of this particular maximum because the electronic structure in the substrate does not depend on x (of course, the electronic structure of the Cu layers near the Co/Cu interface slightly depends on x due to the Co film; see panel (c) in figure 1). The most prominent effect is a reduction of the spin polarization which vanishes for $x = 0.5$. As in the BSF (figure 1), QWSs A and C show no significant intensity maximum for $x = 0.5$. Their intensity drops rapidly upon increasing x, in contrast to that of the Cu-related state D. Further, A and C disperse with x: those maxima with majority spin orientation (C) to higher energies, those with minority spin orientation (A) to lower energies (cf. the guiding lines in figure 2). For example, C disperses by approximately 0.3 eV, A by -0.2 eV. These dispersions are considerably larger than those obtained from the BSF (from figure 1 one can extract for A and C -0.09 eV and 0.04 eV, respectively) which nicely confirms that there is no strict one-to-one correspondence between maxima in the BSF and those in the photoemission spectra. This 'dispersion feature' can be attributed to the broadening of maxima A and C: we recall that the intensity of the photoemission from a QWS shows a maximum right at its binding energy, even if the $k_\perp$-selection is weak for ultrathin films [52]. With increasing x, QWSs become 'less well defined' in energy due to the mixing in of $\boldsymbol{k}_\parallel$-averaged contributions and, thus, a shift in the photoemission maximum via the $k_\perp$-selection may occur.

In order to compare our theoretical results with the experimental ones, we first recall that the experiment has been carried out for a 2.5 ML film. Thus, the positions and intensities of the Co-related peaks might differ from those for a 2.0 ML film due to the excess of 0.5 ML Co. The Cu-related peak D is about 0.5 eV too high in energy compared to experiment which can be explained by shortcomings of the local density approximation used in the *ab initio* calculations. An extension to a non-local density approximation shifts the Cu d bands by about 0.5 eV to lower energies and gives almost perfect agreement with experimental data for Cu(111) [57]. Despite this shortcoming, the theoretical spectrum for $x = 0.45$ corresponds rather well to the experimental one as regards the number of maxima, the intensity relations of the individual maxima, and the spectral shape near E_F. In particular, the relative heights of the intensity peaks from QWS A and that of the Cu d-band peak D agree well and illustrate clearly the failure of describing the experiment by the zero-temperature theory. The most striking difference is that in experiment the majority spectrum exceeds the minority spectrum over the whole energy range. A definitive explanation of this feature is still lacking (for a brief discussion see [28]).

Comparing the results for $x = 0$ with those obtained by Reiser *et al* we find good agreement (cf. figure 2 in [28]). The small differences in the intensity relations between the individual

maxima can be traced back to differences in the parameters—for example, electron and hole lifetimes—and approximations in the transition-matrix elements in the work of Reiser *et al*. Even our spectra for $x \approx 0.45$ obtained within the DLM picture compare well with those of Reiser *et al* for $\langle m(T)\rangle = 0.2\,m(0)$ and moderate correlation length $\Lambda(T)$ obtained within the FLM picture. In summary, the different methods used—the *ab initio* layer-KKR method combined with CPA versus the empirical tight-binding method combined with a real-space cluster approach—give essentially the same results if the spin–spin correlation length $\Lambda(T)$ is small, i.e. if magnetic SRO can be neglected.

Another aspect seems worth mentioning. Our results and those of Reiser *et al* agree with experiment if the net magnetization is rather low: $\langle m(T)\rangle \approx 0.2\,m(0)$ or $x \approx 0.45$, i.e. if T is very close to T_C. The experimental data were recorded at a temperature $T \approx 0.65\,T_C$ which is not too close to T_C. This apparent discrepancy might be explained by imperfections of the film (e.g. defects and interdiffusion) which lower the actual Curie temperature in experiment. As noted in [2], the magnetism of ultrathin films—and therefore their T_C—is rather sensitive to the preparation conditions (see also [58] for Gd/W(110)).

The electron spin polarization obtained from the spectra of figure 2 is shown in figure 3. As mentioned above, the ESP is due solely to exchange splitting. Its global shape can be described as of moderate majority character at the Cu-related emissions (around D), of strong majority character around the Co quantum-well resonance C, and of strong minority character at the Co QWS A. The fact that maximum B shows identifiable intensity only for $x = 0.0$ and 0.1 is also reflected in the ESP. A strong maximum appears for $x = 0.0$ which for $x = 0.1$ shows up as a shoulder and has disappeared for larger x. The ESP of the other states, A, C, and D, can be traced clearly over the whole range of concentration, allowing a discussion of the concentration dependence.

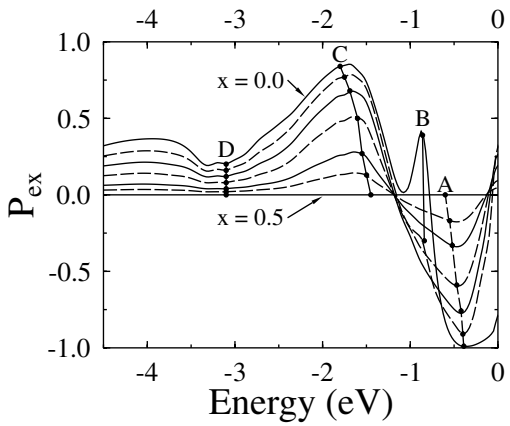

Figure 3. Spin polarization of the photocurrent from 2 ML Co on Cu(001) for normal emission, as obtained from the theoretical spectra of figure 2. For concentrations $x = 0.0, \ldots, 0.5$ the line styles alternate between full (——) and dashed (- - - -). For a better orientation, the polarizations of maxima A–D from figure 2 are indicated by lines to guide the eye and dots. The Fermi energy is 0 eV.

As argued above, the different origins of the states A, C, and D should also be reflected in differences in the temperature dependences of the photo-ESP (cf. the dots in figure 3 and figure 4). In order to achieve quantitative results we fitted the ESP of maxima A, C, and D obtained for the set of concentrations x to a phenomenological power law

$$P_{ex}(x) = P_{ex}(0)[1 - (2x)^b]$$

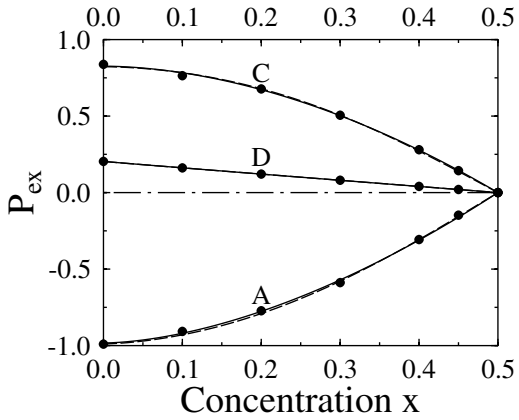

Figure 4. The dependence of the spin polarization P_{ex} for maxima A, C, and D as obtained from figure 3 on the concentration x (dots). The lines show fits of $P_{\mathrm{ex}}(x)$ (——) and of $\widetilde{P}_{\mathrm{ex}}(x)$ (- - - -)—see the text—to the numerical data with the parameters $P_{\mathrm{ex}}(0)$, b, $\widetilde{P}_{\mathrm{ex}}(0)$, and $\tilde{b}$ taken from table 1.

and to

$$\widetilde{P}_{\mathrm{ex}}(x) = \widetilde{P}_{\mathrm{ex}}(0)[(1-x)^{\tilde{b}} - x^{\tilde{b}}]/[(1-x)^{\tilde{b}} + x^{\tilde{b}}]$$

for $x \in [0, \ldots, 0.5]$ (cf. the lines in figure 4). As can be seen from figure 4, the fits are almost perfect, with $\widetilde{P}$ yielding a slightly better fit. The results for $P_{\mathrm{ex}}(0)$, b, $\widetilde{P}_{\mathrm{ex}}(0)$, and $\tilde{b}$ are given in table 1. For A and C we obtain exponents b and $\tilde{b}$ which differ considerably from those for D, i.e. the latter indicate an almost perfect linear dependence over the whole range of concentrations. Critical exponents β for the ESP can be obtained by considering $\lim_{x\to 0.5} \alpha(1-2x)^{\beta}$. Expansion of both $P_{\mathrm{ex}}(x)$ and $\widetilde{P}_{\mathrm{ex}}(x)$ in Taylor series around $x = 0.5$ gives β-values very close to 1 for all three peaks.

Table 1. Parameters describing the dependence of the electron spin polarization for peaks A, C, and D on the concentration x. The values of $P_{\mathrm{ex}}(0)$, b, $\widetilde{P}_{\mathrm{ex}}(0)$, and $\tilde{b}$ have been obtained by fitting the numerical data to $P_{\mathrm{ex}}(x)$ and to $\widetilde{P}_{\mathrm{ex}}(x)$ (see the text) for $x \in [0, \ldots, 0.5]$.

Peak	$P_{\mathrm{ex}}(0)$	b	$\widetilde{P}_{\mathrm{ex}}(0)$	$\tilde{b}$
A	−0.98	1.70	−0.98	1.58
C	0.83	1.84	0.82	1.69
D	0.20	0.98	0.20	0.99

Summing up, the behaviours of the maxima in the BSF, e.g. the dispersion, broadening, and merging, show up also in the spin-resolved photoemission intensities. The spatial origin of individual peaks, Co film or Cu substrate, can be discriminated by considering their ESPs. Also, the theoretical spectra compare reasonably well with their experimental counterparts.

3.3. Magnetic linear dichroism for 2 ML Co on Cu(001)

Magnetic dichroism in angle-resolved photoemission is the change of the photocurrent upon magnetization reversal. In the case of magnetic linear dichroism (MLD) in angular distribution, the incoming light is linearly polarized, in contrast to magnetic circular dichroism, for which the light is circularly polarized. In the standard set-up of MLD, p-polarized light impinges off-normally onto the sample, and the photoelectrons are detected in normal emission. The

surface-parallel magnetization direction $\boldsymbol{M}$ is normal to the reaction plane which is spanned by the directions of the light incidence and the electron emission. For magnetization orientations $\pm\boldsymbol{M}$ one records the photocurrents $I(\pm\boldsymbol{M})$. Or, equivalently, one fixes the magnetization and changes the azimuth of light incidence by 180°, the associated electric field vectors being denoted as $\boldsymbol{p}_+$ and $\boldsymbol{p}_-$. The spin-averaged asymmetry then reads

$$A_{\mathrm{un}} = [I(\boldsymbol{p}_+) - I(\boldsymbol{p}_-)]/[I(\boldsymbol{p}_+) + I(\boldsymbol{p}_-)]$$

where $I(\boldsymbol{p}_\pm)$ are the photocurrents recorded for $\boldsymbol{p}_\pm$ light incidence (cf. also (3)). Note that $I(\pm\boldsymbol{M}, \boldsymbol{p}_\pm) = I(\mp\boldsymbol{M}, \boldsymbol{p}_\mp)$. Since the surface-parallel component of the electric field vector mediates excitations from the $\Delta_5^\pm$ initial states, its surface-normal component allows for excitations of the $\Delta_1^\pm$ initial states. Thus, we expect additional maxima in the MLD spectra with respect to those presented in figure 2.

In contrast to the case of s-polarized light, there is now an ESP component perpendicular to the reaction plane (i.e. parallel to the magnetization) which is due to SOC (see [30] and references therein) and therefore is present even at $x = 0.5$. The 'general rule' of MD states that if in the non-magnetic case ($x = 0.5$) there is a non-zero ESP component and if in the ferromagnetic case ($x < 0.5$) there is a magnetization component parallel to this ESP component, then there will be MD in the ferromagnetic case.

In order to investigate the temperature dependence of the standard MLD for ultrathin films, we performed the same calculations as in section 3.2 but with the light chosen in accordance with the set-up described above. The photoemission spectra $I(\boldsymbol{p}_\pm)$ for $x = 0$ are shown at the top of figure 5. Besides changes in the intensities and the occurrence of the additional maximum E which is due to a Δ_1 initial state, the most important difference from the spectra in figure 2 is the dichroism. The maxima show the same general trends with increasing concentration x

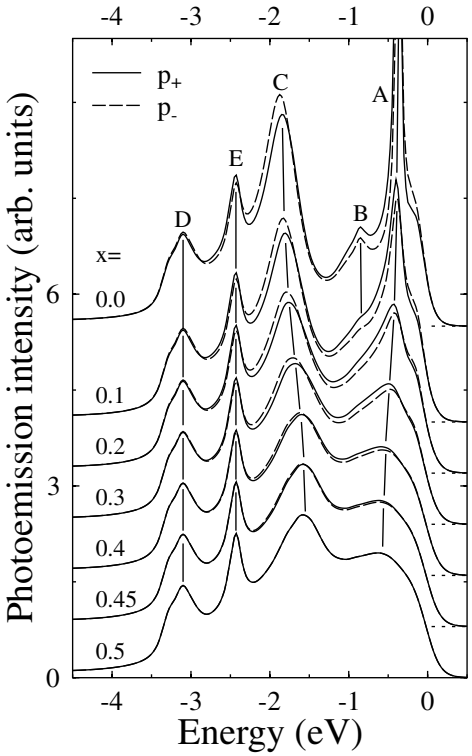

Figure 5. Magnetic linear dichroism (MLD) for 2 ML Co on Cu(001) for normal emission ($\boldsymbol{k}_\parallel = 0$). In the standard set-up for MLD, p-polarized light with photon energy 45 eV impinges at a 45° polar angle onto the surface. For concentrations $x = 0.0, \ldots, 0.5$, the photoemission intensities for incidence directions $\boldsymbol{p}_+$ (——) and $\boldsymbol{p}_-$ (- - - -) are shown, with zero abscissae marked by dotted (· · · · · ·) lines. The maxima discussed in the text are denoted as A–E; almost vertical lines serve as guides to the eye. The Fermi energy is 0 eV.

as in figure 2, in particular broadening and dispersion. Exceptions are features D and E which remain sharp and show no dispersion, both hints of their Cu origin.

In figure 6, the contributions P_{so} and P_{ex} to the ESP are shown. The exchange-induced part P_{ex} shows essentially the same global shape as in figure 3, and the spin–orbit-induced part P_{so} does not vanish for $x = 0.5$. Since for 3d transition metals the spin–orbit interaction is small compared to the exchange interaction, P_{ex} is much larger in absolute value than P_{so}. At energies less than -2.2 eV, P_{so} is virtually independent of x which can be attributed to the fact that emissions in that energy range stem almost exclusively from the Cu substrate.

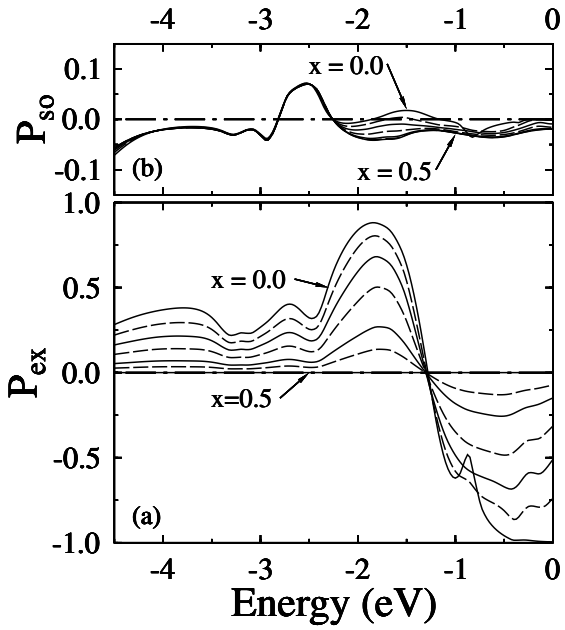

Figure 6. Spin polarizations of the photocurrent from 2 ML Co on Cu(001) for normal emission, as obtained from the theoretical spectra of figure 5. The exchange-related (P_{ex}, (a)) and the spin–orbit-related (P_{so}, (b)) spin polarizations are calculated according to (1) for concentrations $x = 0.0, \ldots, 0.5$, as indicated. Note the different ordinate scales. The Fermi energy is 0 eV.

We now discuss the x-dependence of the asymmetries which have been introduced in section 2.2. In figure 7 the spin-averaged (A_{un}), the spin–orbit-related (A_{so}), and the exchange-related (A_{ex}) spin asymmetries are shown. Because the dichroism and P_{so} are comparably small (both A_{un} and P_{so} are less than 10% in absolute value), $A_{ex} = P_{ex} + P_{so}A_{un}$ coincides almost perfectly with P_{ex} (cf. panel (a) in figure 6). As mentioned above, for $x = 0.5$ we have $P_{ex} = A_{ex} = 0$ and thus $A_{so} = P_{so}$. Upon decreasing x, P_{ex} becomes mixed into $A_{so} = P_{so} + P_{ex}A_{un}$. Therefore, one observes a rather strong effect on A_{so} at energies at which A_{un} is changed considerably, for example at energies higher than ≈ -2.5 eV and in particular at -0.5 eV (note that this is the energy range of Co-related emissions). At lower energies, A_{so} is virtually independent of x because in this energy range A_{un} is also very small.

We now briefly analyse our spin-resolved results with regard to relations between the spin asymmetries and the ESPs. For example, at those energies where $A_{un} = 0$, both A_{so} and A_{ex} are in general non-zero and show negative as well as positive values. Further, one could hope that A_{ex} would govern the behaviour of the other asymmetries. But A_{ex} shows a general $+/-$ shape which is reflected neither in A_{so} nor in A_{un}. Summarizing briefly, we would like to emphasize

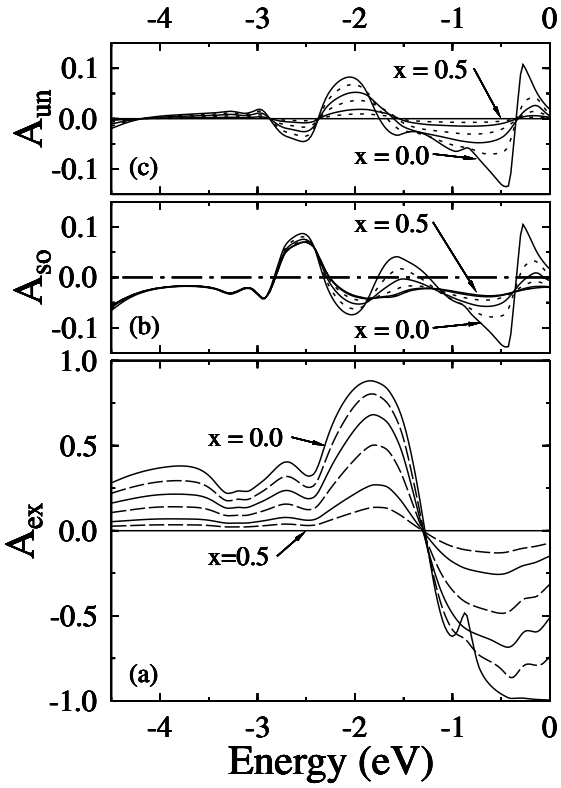

Figure 7. Asymmetries of the photocurrent from 2 ML Co on Cu(001) for normal emission, as obtained from the theoretical spectra of figure 5. The exchange-related (A_{ex}, (a)), the spin–orbit-related (A_{so}, (b)), and the spin-averaged (A_{un}, (c)) asymmetries are calculated according to (3) for concentrations $x = 0.0, \ldots, 0.5$, as indicated. Note the different ordinate scales. The Fermi energy is 0 eV.

that MD and spin-resolved photoemission complement each other [50]. Therefore, it appears desirable from our point of view to perform a more complete experiment or calculation, e.g. one based on spin-resolved instead of spin-averaged MD.

Finally, the 'critical exponents' of the spin asymmetries are discussed very briefly. As for P_{ex} in the case of s-polarized light, we find a perfect linear dependence on x of A_{un} for maxima D and E which again evidences the bulk origin of the respective initial states. For states A and C the x-dependence is monotonic but cannot be fitted well with a power law.

4. Conclusions

For the prototypical system 2 ML Co on Cu(001) we carried out relativistic *ab initio* layer-KKR calculations in order to investigate the temperature dependences of the electronic structure and spin-resolved (dichroic) photoemission within the disordered local moment picture.

In particular, for quantum-well states in the Co film, our results show distinct dispersion, broadening, and in some cases merging with temperature in the Bloch spectral function and in the photocurrent. In contrast, Cu-derived maxima show no dispersion and significantly different dependences of both the electron spin polarization and the magnetic linear dichroism.

We would like to stress that this can be used in experiments to discriminate between Cu- and Co-derived states. Further, the spin-resolved photoemission intensities compare well with experimental data and other theoretical ones, the latter obtained within the fluctuating local moment picture.

As an extension of the present study one might think of treating the spin–spin correlation within the FLM picture, i.e. taking into account magnetic short-range order. This can be done for example within the real-space KKR approach. We hope that the present study will prompt experimental investigations of the temperature dependence of magnetic dichroism in valence band photoemission.

Acknowledgments

Fruitful discussions with Yonko T Millev are gratefully acknowledged. We are also grateful to Arthur Ernst for help with the self-consistent computations.

References

[1] Campagna M and Rosei R (ed) 1990 *Photoemission and Absorption Spectroscopy of Solids and Interfaces with Synchrotron Radiation* (Amsterdam: North-Holland)
[2] Schneider C M, Bressler P, Schuster P, Kirschner J, de Miguel J J and Miranda R 1990 *Phys. Rev. Lett.* **64** 1059
[3] Crangle J 1955 *Phil. Mag.* **46** 499
[4] Huang F, Kief M T, Mankey G J and Willis R F 1994 *Phys. Rev.* B **49** 3962
[5] Duke C B and Laramore G E 1970 *Phys. Rev.* B **2** 4765
[6] Laramore G E and Duke C B 1970 *Phys. Rev.* B **2** 4783
[7] Nolting W, Braun J, Borstel G and Borgiel W 1990 *Phys. Scr.* **41** 601
[8] Braun J, Nolting W and Borstel G 1991 *Surf. Sci.* **251/252** 22
[9] Braun J, Borstel G and Nolting W 1992 *Phys. Rev.* B **46** 3510
[10] Chen C 1993 *Phys. Rev.* B **48** 1318
[11] Soven P 1967 *Phys. Rev.* **156** 809
[12] Faulkner J S and Stocks G M 1980 *Phys. Rev.* B **21** 3222
[13] Durham P J, Gyorffy B L and Pindor A J 1980 *J. Phys. F: Met. Phys.* **10** 661
[14] Gonis A 1992 *Green Functions for Ordered and Disordered Systems (Studies in Mathematical Physics vol 4)* (Amsterdam: North-Holland)
[15] Weinberger P 1990 *Electron Scattering Theory of Ordered and Disordered Matter* (Oxford: Clarendon)
[16] Gyorffy B L, Pindor A J, Staunton J, Stocks G M and Winter H 1985 *J. Phys. F: Met. Phys.* **15** 1337
[17] Staunton J, Gyorffy B L, Pindor A J, Stocks G M and Winter H 1985 *J. Phys. F: Met. Phys.* **15** 1387
[18] Durham P J 1981 *J. Phys. F: Met. Phys.* **11** 2475
[19] Durham P J, Staunton J and Gyorffy B L 1984 *J. Magn. Magn. Mater.* **45** 38
[20] Weinberger P, Dirl R, Boring A M, Gonis A and Freeman A J 1988 *Phys. Rev.* B **37** 1383
[21] Haines E M, Heine V and Ziegler A 1985 *J. Phys. F: Met. Phys.* **15** 661
[22] Haines E M, Heine V and Ziegler A 1986 *J. Phys. F: Met. Phys.* **16** 1343
[23] Haines E M 1985 *J. Comput. Phys.* **60** 353
[24] Gollisch H and Feder R 1989 *Physica* B **161** 169
[25] Gollisch H and Feder R 1989 *Solid State Commun.* **69** 579
[26] Gollisch H and Feder R 1990 *Solid State Commun.* **76** 237
[27] Delgadillo I, Gollisch H and Feder R 1994 *Phys. Rev.* B **50** 15 808
[28] Reiser D, Henk J, Gollisch H and Feder R 1995 *Solid State Commun.* **93** 231
[29] Clemens W, Kachel T, Rader O, Vescovo E, Blügel S, Carbone C and Eberhardt W 1992 *Solid State Commun.* **81** 739
[30] Feder R and Henk J 1996 *Spin–Orbit Influenced Spectroscopies of Magnetic Solids (Springer Lecture Notes in Physics vol 466)* ed H Ebert and G Schütz (Berlin: Springer) p 85
[31] Sirotti F, Panaccione G and Rossi G 1995 *Phys. Rev.* B **52** R17 063
[32] Schmitz D, Rader O, Carbone C and Eberhardt W 1996 *Phys. Rev.* B **54** 15 352
[33] Alders D, Vogel J, Levelut C, Peacor S D, Hibma T, Sacchi M, Tjeng L H, Chen C T, van der Laan G, Thole B T and Sawatzky G A 1995 *Europhys. Lett.* **32** 259

[34] Weber W, Bischof A, Allenspach R, Back C, Fassbender J, May U, Schirmer B, Jungblut R, Güntherodt G and Hillebrands B 1996 *Phys. Rev.* B **54** 4075
[35] Ramsperger U, Vaterlaus A, Pfäffli P, Maier U and Pescia D 1996 *Phys. Rev.* B **53** 8001
[36] Fassbender J, Allenspach R and Dürig U 1997 *Surf. Sci.* **383** L742
[37] Perdew J P and Wang Y 1992 *Phys. Rev.* B **45** 13 244
[38] Niklasson A M N 1999 private communication
[39] Henk J, Scheunemann T, Halilov S V, Tamura E and Feder R 2000 *omni2k—Fully Relativistic Electron Spectroscopy Calculations*
The computer code is available from the authors. Electronic address: henk@mpi-halle.mpg.de.
[40] Ebert H, Freyer H and Deng M 1997 *Phys. Rev.* B **56** 9454
[41] Tamura E 1996 private communication
[42] Bruno E and Ginatempo B 1997 *Phys. Rev.* B **55** 12 946
[43] Chen C 1990 *Phys. Rev. Lett.* **64** 2176
[44] Chen C 1991 *Int. J. Mod. Phys.* B **5** 1147
[45] Chen C 1994 *Phys. Rev. Lett.* **73** 1982
[46] Chen C 1990 *Phys. Rev.* B **41** 5031
[47] Aryasetiawan F and Gunnarson O 1998 *Rep. Prog. Phys.* **61** 237
[48] Hedin L 1999 *J. Phys.: Condens. Matter* **11** R489
[49] Ernst A and Bruno P 2001 *GW* approximation: KKR implementation, to be published
[50] Venus D, Kuch W, Lin M T, Schneider C M, Ebert H and Kirschner J 1997 *Phys. Rev.* B **55** 2594
[51] Rampe A, Güntherodt G, Hartmann D, Henk J, Scheunemann T and Feder R 1998 *Phys. Rev.* B **57** 14 370
[52] Henk J and Johansson B 1999 *J. Electron Spectrosc. Relat. Phenom.* **105** 187
[53] Dederichs P H, Wildberger K and Zeller R 1997 *Physica* B **237+238** 239
[54] Paggel J J, Miller T and Chiang T C 1999 *Science* **283** 1709
[55] Henk J, Scheunemann T, Halilov S and Feder R 1996 *J. Phys.: Condens. Matter* **8** 47
[56] Kuch W, Lin M T, Meinel K, Schneider C M, Noffke J and Kirschner J 1995 *Phys. Rev.* B **51** 12 627
[57] Courths R, Lau M, Scheunemann T, Gollisch H and Feder R 2000 From the Shockley surface state on Cu(111) to sp-like surface resonances on Cu_3Au(111) *Phys. Rev.* B submitted
[58] Farle M, Baberschke K, Stetter U, Aspelmeier A and Gerhardter F 1993 *Phys. Rev.* B **47** 11 571